Received: 28 April 2022 | Revised: 02 June 2022 | Accepted: 10 June 2022
DOI: 10.22034/ecc.2022.344547.1479
Eurasian Chemical Communications
SAMI

FULL PAPER

Investigation of the electrical, compositional, and magnetic features of hybrid lead oxide nanocomposites

Ahmed K. Abass* | **Wadhah Naji Jassim Al Sieadi** | **Abdul Karim M.A. Al-Sammarraie**

Department of Chemistry, College of Science, University of Baghdad, Baghdad, Iraq

***Corresponding Author:**
Ahmed K. Abass
Email: ahmedkadhim1975@gmail.com
Tel.:+9647808234906

Three novel nanocomposites were synthesized using the co-precipitation method: lead oxide (β-PbO-massicot), lead ferrite ($PbFe_8O_{18}$), and lead ferrite polypyrrole ($PbFe_2O_7$:PYY). The magnetometer with vibrating-sample-VSM, thermal stability via gravimetry analysis-TGA, Raman, scanning field emission scanning electron microscopy-FESEM, and x-ray diffraction spectroscopy-XRD were used to characterize the nanocomposites. According to XRD measurements, β-PbO and $PbFe_2O_7$:PYY have an orthorhombic crystal structure, while $PbFe_8O_{18}$ has a monoclinic structure. To calculate crystallite size, the Scherrer model was utilized, which provided a significant value in β-PbO and a small value in $PbFe_2O_7$:PYY. Raman's research revealed a significant change in the composite structure, indicating the creation of nanomaterials. According to the AC conductivity tests, β-PbO has a lower conductivity than $PbFe_8O_{18}$, however, $PbFe_2O_7$:PYY has a higher conductivity. When assessed using the VSM technique, $PbFe_8O_{18}$ has higher Ms values.

KEYWORDS

Organic and inorganic hybrid nanocomposites; lead oxides; iron oxides; polypyrrole.

Introduction

Selectivity and activity are two features that organo-inorganic hybrid compounds can have [1,2]. They promote CO_2 adsorption and conductivity, among other physicochemical features. They also have more active site types, more active site exposure, and altered reaction pathways [3,4]. Because of their many phases, lead oxides are intriguing substances. PbO (α, β and amorphous), Pb_2O_3, Pb_3O_4, and PbO_2 (α, β and amorphous) are the four basic kinds [3,4]. PbO is polymorphic and has a large band gap. The yellow -PbO is one of these two forms and it is stable at temperatures over 425 °C. The red α-PbO, which is stable at low temperatures, is the second form. At around 490 °C, the α-PbO phase transforms to β-PbO [5,6]. The high-temperature yellow form, on the other hand, may persist at normal temperature. PbO is a high-dielectric-constant transparent conducting oxide (TCO) [7]. Furthermore, it is a substance with a high refractive index.

Hematite (Fe_2O_3) has a 2.1 eV of band gap and it is a semiconductor compound of n-type. As an inexpensive semiconductor material, iron oxide is extensively used in gas sensing applications, catalyzed reactions, conversion methods of solar energy, batteries of lithium ion, purification processes, splitting of water, and bio-medicine claims among further applications [8,9]. Due to their unique properties and potential applications, conductive polymers have attracted a lot of attention in the last three decades [10,11]. Nanocomposites made of conductive polymers and metal oxides are becoming

increasingly popular in a number of applications. Previous research has shown that metal oxides can raise the dielectric, electrical, mechanical, and optical characteristics of conductive polymers [12].

Conductive polymers having conjugated double bonds have recently attracted a lot of interest for application in conductive thin films. Polypyrrole (PPy) has sparked particular attention because to its excellent environmental stability, ease of synthesis, and high electrical conductivity [13]. Chemical oxidation of pyrrole (Py) or electrochemical polymerization techniques can be used to synthesize PPy. Many parameters can influence PPy characteristics, including synthesis technique, polymerization rate, solvent nature, and reaction medium pH [14]. The chemical polymerization of pyrrole is particularly essential, since it allows for the manufacture of PPy on a larger scale [15]. The aim of the study is to synthesize novel nanocomposites to improve the physical features of lead oxide, as well as to investigate the structures of nanocomposites created using a new microemulsion process.

Experimental

First step: synthesis of lead oxide (PbO)

10 molars of sodium hydroxide were prepared by dissolving 40 gm of it in 100 mL of deionized water. Then, lead nitrate [Pb $(NO_3)_2$] solution was prepared by dissolving 11.871 g of lead nitrate in 100 mL of deionized water through 30 minutes. The above solution of sodium hydroxide was added from the burette dropwise to the nitrate solution at a pH = 8 and a temperature of 60 °C. The appearance of a white foggy solution indicates the formation of lead hydroxide and the stirring was continued for 4 hours. The precipitate was dried for 12 hours at a temperature of 110 °C, and then was burned at a temperature of 600 °C and ground in a ceramic mortar to obtain a very fine powder.

Second step: synthesis of lead iron oxide ($PbFe_8O_{18}$)

By dissolving 40 gm of sodium hydroxide in 100 mL of deionized water 10 molars of sodium hydroxide were yielded. Then, 5.9355 gm of lead nitrate [Pb $(NO_3)_2$] and 10.1197 gm of iron nitrate [Fe $(NO_3)_3.9H_2O$] were dissolved in 100 mL of deionized water to prepare a lead iron nitrate solution. At pH=8and 60 °C, the sodium hydroxide solution was dropped into the nitrate solution from the burette. The formation of a dark brown solution indicated the production of lead iron hydroxide and stirring was continued for another four hours. The precipitate was dried for 12 hours at 110 °C, then calcined at 600 °C and was grounded into a fine powder in a ceramic mortar.

Third step: synthesis of lead iron oxide polypyrrole ($PbFe_2O_7$:PYY)

0.2884 gm of Sodium dodecyl sulfate (SDS) was dissolved in 100 mL of deionized water at 60 °C until a clear and homogeneous solution was reached. 0.81102 gm of ferric chloride ($FeCl_3$) was dissolved in the above solution and the mixture was placed at a temperature of (0-4) °C. Newly distilled pyrrole was added to the mixture drop by drop and at the same time, 3 gm of lead iron oxide was added and stirring was continued for 4 hours. Then, the precipitate was washed with ethanol and with deionized water many times.

Results and discussion

FESEM analysis

Field-emission scanning electron microscopy was utilized to investigate the surface morphology of the produced nanomaterials as in Figure 1. The shape of PbOmassicot with the stacked folded sheet's structure created by the co-precipitation approach and $PbFe_8O_{18}$ take the large lumps of small granules. The scanning pictures designate a relative uniformity distribution of particle size and the

particles seem to be sphere-shaped and agglomerative due to a variety of attractive interactions such as coulomb and Vander Waal attractions, hydrogen bonding as well as physical contact between the nanoparticles. $Pb_3Fe_2O_7$: PYY is a folded paper-like material with very minute grains.

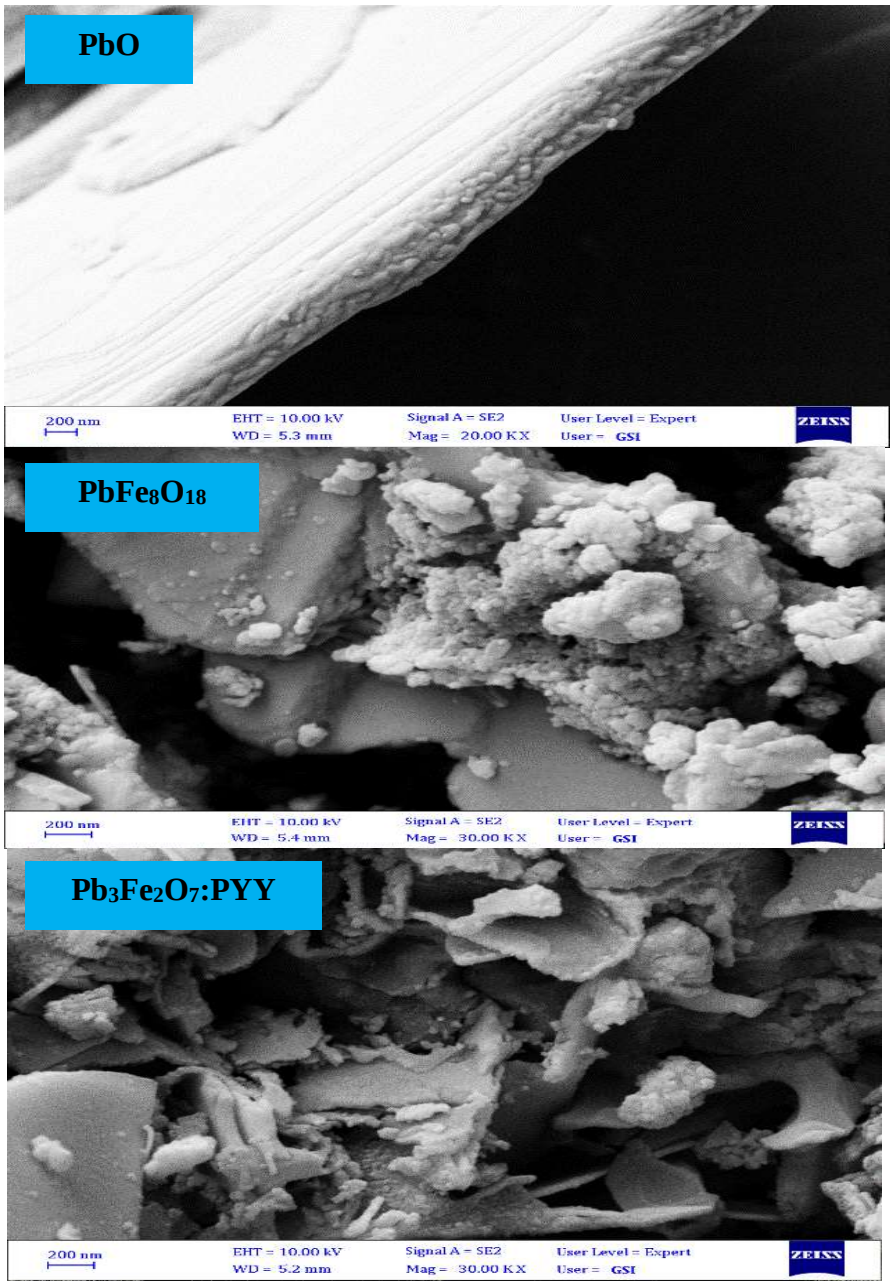

FIGURE 1 FESEM images of β-PbO, $PbFe_8O_{18}$ and $Pb_3Fe_2O_7$:PYY

XRD analysis

Figure 2 shows the XRD patterns of the synthesized lead oxide and its nanocomposites. PbO has thirty diffractions at maxima of 2θ (28.5592) and d-spacing 3.12558, $PbFe_8O_{18}$ has twenty diffractions at maxima 2θ (29.0561), and d-spacing 3.07326, whereas $Pb_3Fe_2O_7$: PYY has twenty-three diffractions at maxima of 2θ (29.8132) and d-spacing 2.99691.

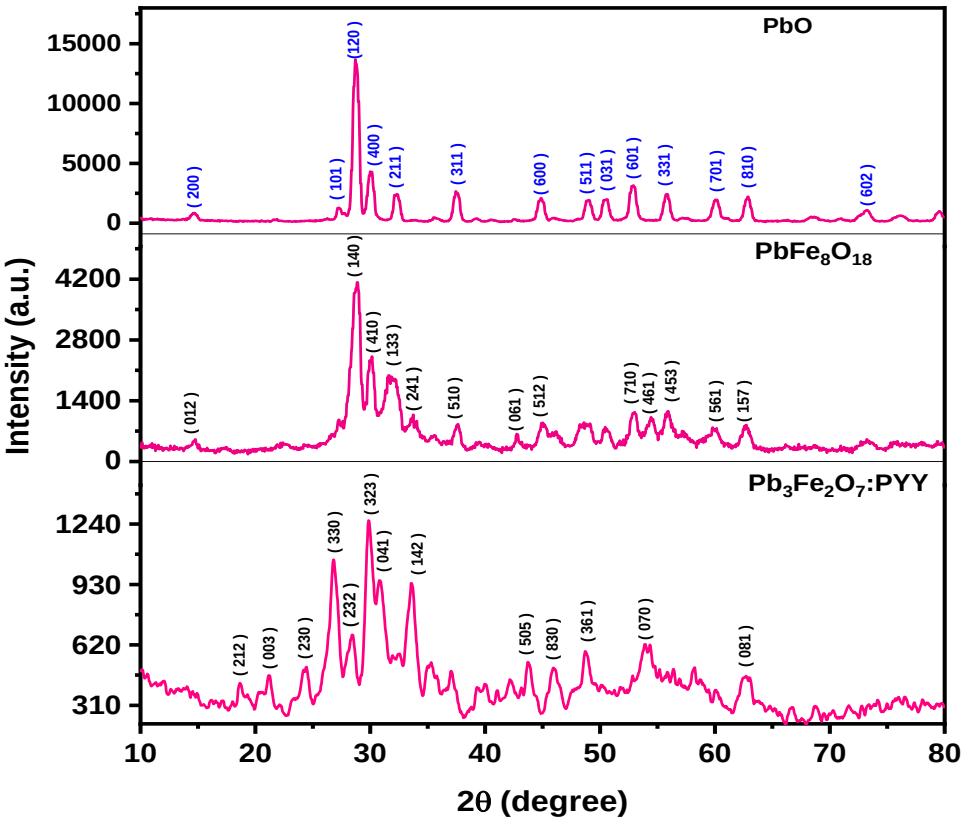

FIGURE 2 XRD diffractions of β-PbO, $PbFe_8O_{18}$, and $Pb_3Fe_2O_7$:PYY

To identify the lead oxide XRD peaks, (Crystallographic Database Code Amcsd 0010011) was employed [16-21]. Peaks at 2θ (29.1, 30.38, and 53.14) had been discovered to be appropriately cataloged to β-PbO (massicot kind) which had a crystal form of orthorhombic system. Miller indices were estimated via utilizing phase identification programs of XRD and specified at the XRD peaks. In XRD diffractograms of $PbFe_8O_{18}$ nanoparticles, 2θ at (29.1, 30.3, and 38) refers to lead oxide (PbO) of massicot type and peaks at (2θ 27.5, 32.01, and 49.11) belonged to iron oxide (Fe_8O_{17}) of schwertmannite type according to Database numbered 0017807 of acta crystallographic.

From the XRD phase identification for the $Pb_3Fe_2O_7$:PYY nanocomposite at 2θ (26.85, 30.85, and 33.6), lead oxide possessed minium kind (Pb_3O_4)whereas iron oxide was hematite type (Fe_2O_3) by indexing at 2θ (26.85, 28.4, and 29.9). It has already been noted that a broader peak at 2θ between 20–28° corresponds to the distinctive peak of PYY [22].

Table 1 indicates the decrease in the density of unit cell due to the increase in the number and size of unit cells. The contact between the segments was discovered to be the cause of the association between crystal deformations and dislocation density [23]. PbO possessed greater crystallinity, while $Pb_3Fe_2O_7$:PYY had lower crystallinity, due to the increased amorphousness for amorphous Fe_2O_3 and amorphous polypyrrole [24-26].

TABLE 1 Crystallographic variables of β-PbO, $PbFe_8O_{18}$, and $Pb_3Fe_2O_7$: PYY nanocomposites

Nanoparticle	Dp (nm)	Dislocation density (nm^{-2})	No. of Unit cell	Patterson Space Group	Cell parameters α	β	γ	a	b	c	Cell volume	Density ($g.cm^{-3}$)	Crystallinity (%)	Cell volume
PbO	26.0299	0.0021	35657	Pmmm	90.00	90.00	90.00	12.13	6.42	3.35	260.49	9.96	71.60	260.49
$PbFe_8O_{18}$	17.9060	0.0038	11279	P2/m	90.00	115.30	90.00	13.47	12.81	15.16	2365.09	5.11	46.10	2365.09
$Pb_3Fe_2O_7$: PYY	11.4954	0.0082	6828	Pmmm	90.00	90.00	90.00	18.17	11.90	12.56	2717.82	3.53	29.51	2717.82

Raman identification

Raman spectra collected over a wide spectral range (60 to 3500) cm^{-1} indicated distinct massicot peaks at (87.1764, 142.4454, 290.0771, and 383.8443) cm^{-1}, as displayed in Figure 3. The Raman bands are consistent with previous references [27]. Changes in the methodology and the location of holes in the unit cell might cause the relative positions of the peaks to shift [28]. Figure 4 depicts the loss of massicot peaks (87.1764, 142.4454, and 290.0771) cm^{-1} and the creation of additional peak at 131.0657 cm^{-1}, as well as weak schwertmannite peaks at (219.9227, 319.3932, and 545.9959) cm^{-1}, demonstrating the formation of the $PbFe_8O_{18}$.

According to the IRUG Filename: RMP00042 database, the peak at 89.7375, 138.424, and 262.6492 cm^{-1} belongs to lead oxide of the minium kind. The peak at 407.9952 and 498.9260 cm^{-1} represents hematite, whereas the peaks at 1060 and 1368cm^{-1} indicate polypyrrole [29]. Findings which were acquired by using the Raman analysis are comparable to those obtained using the XRD technique.

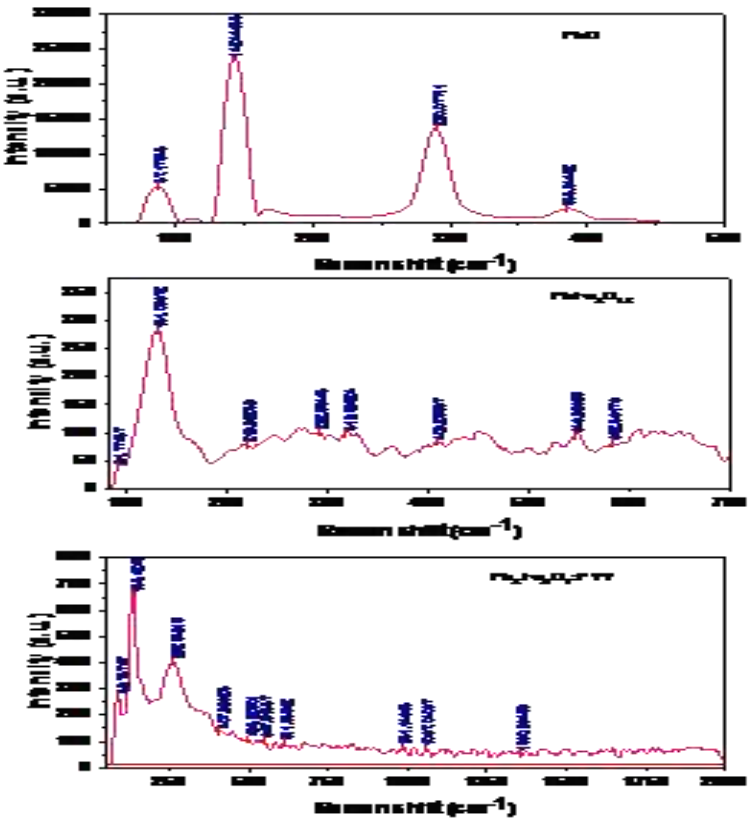

FIGURE 3 Raman spectra of β-PbO, $PbFe_8O_{18}$ and $Pb_3Fe_2O_7$:PYY

Conductivity tests

The dielectric and electrical conductivity behavior of the prepared nanomaterials were depicted in Figure 4. A frequency range of 50 Hz to 1 MHz was employed in the experiment. In the low-frequency domain, β- PbO nanoparticles exhibit minimal conductivity, which lasts up to 40 kHz, although $PbFe_8O_{18}$ and $Pb_3Fe_2O_7$:PYY nanoparticles have conductivity up to 3.5 kHz and 2.5 kHz, respectively. $Pb_3Fe_2O_7$:PYY exhibited a greater conductivity of 17.4564 x 10^{-4} Sm^{-1} than β-PbO, which was 18.281 x 10^{-7} Sm^{-1}., as observed in Table 2.

Because enormous charge carriers of Fe_2O_3, Fe_8O_{18}, and polypyrrole are produced as a result of their own adequate energy, the conductivity of synthesized nanocomposites rises with frequency, especially at high frequencies. A non-continuous leap transition charge carrier or its reorientation between local levels of crystal boundaries increases the frequency of the electric field applied to the samples [30].

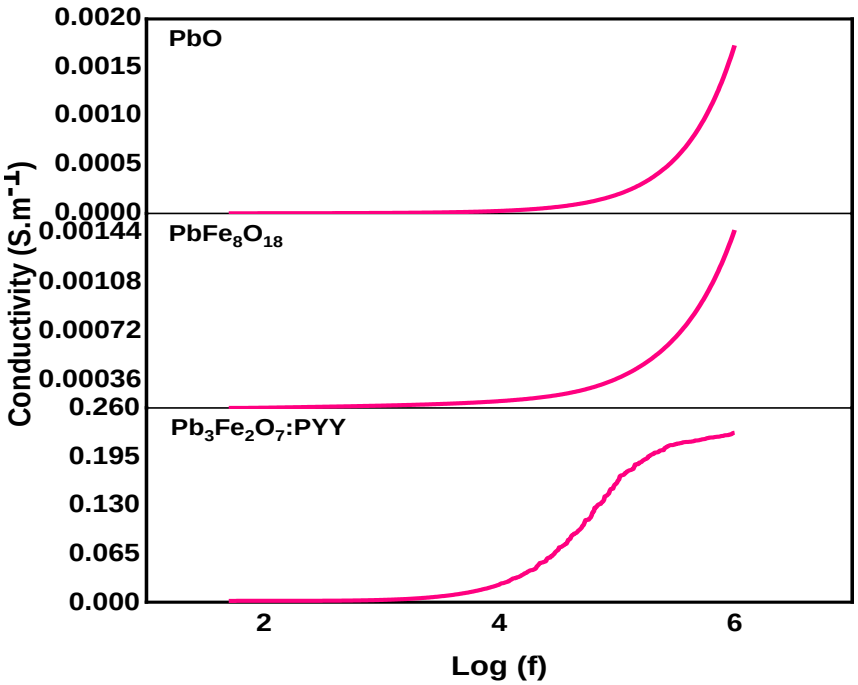

FIGURE 4 Conductivity measurements of β-PbO, $PbFe_8O_{18}$ and $Pb_3Fe_2O_7$:PYY

TABLE 2 Conductivity values of β-PbO, $PbFe_8O_{18}$ and $Pb_3Fe_2O_7$:PYY

Nanomaterial	Conductivity (Sm^{-1})	
	50 Hz (x10^{-3})	1 MHz (x10^{-3})
β-PbO	0.0018	1.7280
$PbFe_8O_{18}$	0.1002	1.3985
$Pb_3Fe_2O_7$:PYY	0.0017	200.2658

Thermogravimetric studies

With a temperature range of (30-800) °C and a flow rate of 40 mL/min, the thermodynamic features and thermal stability of produced nanocomposites were examined using thermogravimetric analysis. The TGA graph between temperature and weight loss, as displayed in Figure 5, demonstrated the thermal behavior of the nanocomposites. β-PbO and $PbFe_8O_{18}$ nanocomposites were demonstrated to be exceptionally stable and did not break down appreciably across a wide temperature range, whereas $Pb_3Fe_2O_7$:PYY showed only the moderate thermal stability.

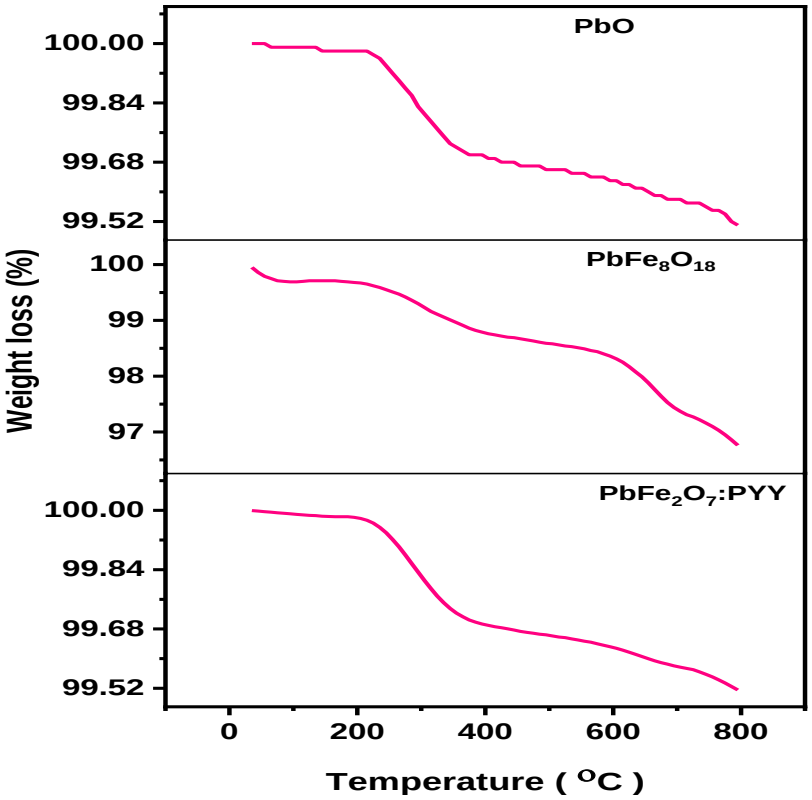

FIGURE 5 Thermograms of β-PbO, $PbFe_8O_{18}$ and $Pb_3Fe_2O_7$:PYY

The thermal behavior of nanocomposites includes two main stages: the initial stage is connected with a relatively tiny percentage of humidity loss, with $PbFe_8O_{18}$ losing more than others due to its wide pore diameter, whereas β-PbO had tiny porosity because of its small diameter. The adsorbed oxygen molecules are released in the second stage, and $PbFe_8O_{18}$ frees much more humidity in both temperature series than other nanoparticles. The beginning, final temperature, weight loss, and onset temperature were illustrated in Table 3. Tables 4, 5, and 6 provide the thermogravimetric functions of β-PbO, $PbFe_8O_{18}$, and $Pb_3Fe_2O_7$:PYY for the various temperature ranges. $Pb_3Fe_2O_7$:PYY had the lowest activation energy (Ea), whereas β-PbO had the highest. The change in entropy (S) was increased by adding other components to β-PbO as composites due to the rise in amorphous nature and porosity (polypyrrole and iron oxide). Likewise, the thermal processes occurred spontaneously due to the minus sign of the Gibbs free energy.

TABLE 3 Thermogravimetric data of β-PbO, $PbFe_8O_{18}$ and $Pb_3Fe_2O_7$:PYY

Compound	Initial temperature (°C)	Ending temperature (°C)	Weight loss (%)	Weight loss (mg)	Onset temperature (°C)
β-PbO	27.9200	800.1000	0.5000	0.0390	237.8100
	31.2200	799.9400	3.2930	0.0880	
	31.2200	90.5300	0.3080	0.0080	55.9200
$PbFe_8O_{18}$	90.5300	435.7900	0.9900	0.0270	227.2500
	435.7900	707.8700	1.3500	0.0360	611.1600
	707.8700	799.9400	0.6450	0.0170	767.4100
$Pb_3Fe_2O_7$:PYY	30.8200	799.9300	11.5900	0.7170	378.6700

TABLE 4 Thermogravimetric quantities of massicot (β-PbO) at a set of temperatures

Temperature set (°C)	ΔE_a (J/mol)	ΔH (J/mol)	ΔS ($JK^{-1}mol^{-1}$)	ΔG (J/mol)
220-350	43904.8800	39499.9600	197.2300	-64996.0000
360-560	-4577.6400	-8982.5600	194.9400	-145024.0000

TABLE 5 Thermogravimetric quantities of $PbFe_8O_{18}$ at a set of temperatures

Temperature set (°C)	ΔE_a (J/mol)	ΔH (J/mol)	ΔS ($JK^{-1}mol^{-1}$)	ΔG (J/mol)
250-380	14042.9300	9638.0100	196.3100	-106583.0000
435-585	-4025.2400	-8430.1600	193.5600	-167792.0000
618-688	48107.4200	43702.5000	192.6500	-133295.0000

TABLE 6 Thermogravimetric quantities of $Pb_3Fe_2O_7$:PYY at a set of temperatures

Temperature set (°C)	ΔE_a (J/mol)	ΔH (J/mol)	ΔS ($JK^{-1}mol^{-1}$)	ΔG (J/mol)
100-345	9959.2900	5554.3700	196.8900	-103113.0000

VSM measurements

The VSM approach was used to test the magnetic performance of nanocomposites at moderate temperatures using hysteresis graphs of the samples at a set of fields from -10000 to 10000. It was found that massicot is paramagnetic and the magnetic material (schwertmannite) in $PbFe_8O_{18}$ produces more magnetism than massicot as noticed from the rising in the magnetization with the applied magnetic field, the data were illustrated in Figure 6.

Sublattices in magnetic materials contain two magnetic moments, one per each. Consequently, even if the moments have a similar sign, they do not eliminate completely, leading to a nonzero net moment. Between the ferro and antiferromagnetic states, the ferrimagnetic state occurs. As a result, a ferrimagnet's magnetic properties are identical to those of a ferromagnet at any temperature. The magnetic characteristics of $Pb_3Fe_2O_7$: PYY core shells are due to the Fe_2O_3 core. A little amount in the Ms value for $Pb_3Fe_2O_7$:PYY core shells further indicates the existence of the polypyrrole shell on the Fe_2O_3 core surface [31,32]. Table 7 illustrates that the saturation magnetization (Ms) of β-PbO is 0.01277 emu/g, whereas the Ms of $PbFe_8O_{18}$ core-shell is 1.42604 emu/g.

TABLE 7 Magnetic parameters of β-PbO, $PbFe_8O_{18}$ and $Pb_3Fe_2O_7$:PYY

Compound	Ms	Mr (x 10^{-4})	Hc (x 10^{-4})
PbO	0.0128	4.6819	0.0804
$PbFe_8O_{18}$	1.4260	852.0000	4.4065
$Pb_3Fe_2O_7$: PYY	0.0182	1.0000	0.0095

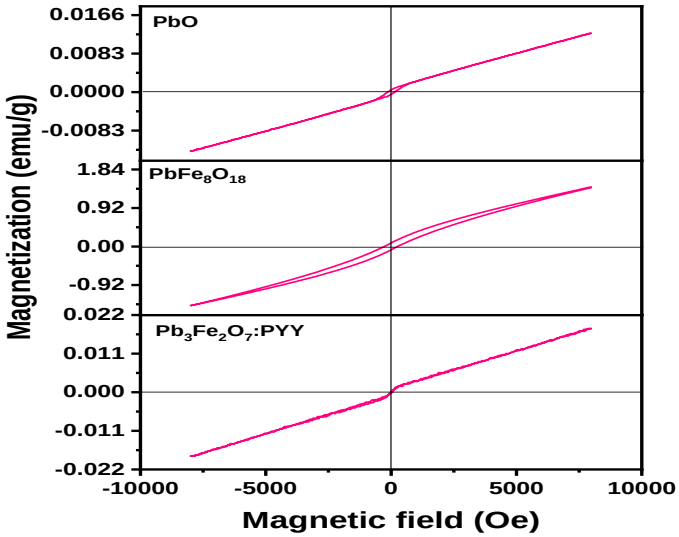

FIGURE 6 Vibrating sample magnetometry measurements of β-PbO, $PbFe_8O_{18}$ and $Pb_3Fe_2O_7$:PYY

Conclusion

A co-precipitation approach was used to synthesize lead oxide and its new nanocomposites. According to the XRD analysis, the lead oxide was massicot type in PbO and in $PbFe_8O_{18}$, whereas the iron oxide was schwertmannite type. In $Pb_3Fe_2O_7$:PYY, lead oxide had minium type phase, while iron oxide had a hematite type.It is worth to note that nanocomposites' surface shape altered considerably which revealed that synthesis was successful. According to Raman spectra, nanocomposites display a wavelength shift, and the results were comparable to XRD investigations. As frequency increased, conductivity increased, and the $Pb_3Fe_2O_7$:PYY had a higher conductivity. Due to the presence of more magnetic hematite, VSM analysis revealed that $PbFe_8O_{18}$ has a strong magnetism, and TGA study revealed that nanocomposites are stable.

Acknowledgments

The authors are grateful to Al-Qadisiyah University's Chemistry Department for finishing the laboratory synthesis of nanomaterials, Baghdad University's Chemistry Department, and Tehran University for different characterizations.

Orcid:

Ahmed K. Abass:
https://orcid.org/0000-0002-4243-4793

References

[1] C. Sanchez, B. Julián, P. Belleville, M. Popall, *J. Mater. Chem.*, **2005**, *15*, 3559. [Crossref], [Google Scholar], [Publisher]
[2] M. Faustini, L. Nicole, E. Ruiz-Hitzky, C. Sanchez, *Adv. Funct. Mater.*, **2018**, *28*, 1704158. [Crossref], [Google Scholar], [Publisher]
[3] Z. Jiang, Y. Wang, X. Zhang, H. Zheng, X. Wang, Y. Liang, *Nano Res.*, **2019**, *12*, 2330-2334. [Crossref], [Google Scholar], [Publisher]
[4] H. Li, C. Chen, D. Yan, Y. Wang, R. Chen, Y. Zou, S. Wang, *J. Mater. Chem.*, **2019**, *7*, 23432-23450. [Crossref], [Google Scholar], [Publisher]
[5] M. Salavati-Niasari, F. Mohandes, F. Davar, *Polyhedron*, **2009**, *28*, 2263–2267. [Crossref], [Google Scholar], [Publisher]
[6] L. Zhang, F. Guo, X. Liu, J. Cui, Y. Qian, *J. Cryst. Growth*, **2005**, *280*, 575–580. [Crossref], [Google Scholar], [Publisher]
[7] B.T. Lu, J.L. Luo, Y.C. Lu, *Electrochim. Acta*, **2013**, *87*, 824–838. [Crossref], [Google Scholar], [Publisher]
[8] A. Miri, M. Sarani, A. Hashemzadeh, Z. Mardani, M. Darroudi, *Green Chem. Lett. Rev.*,

2018, *11*, 567–572. [Crossref], [Google Scholar], [Publisher]
[9] Y. Jiao, Y. Liu, F. Qu, X. Wu, *Cryst. Eng. Comm.*, **2014**, *16*, 575–580. [Crossref], [Google Scholar], [Publisher]
[10] K. Gupta, P.C. Jana, A.K. Meikap, *Synth. Met.*, **2010**, *160*, 1566–1573. [Crossref], [Google Scholar], [Publisher]
[11] G. Inzelt, *Conducting Polymers: Monographs in Electrochemistry*, Springer Berlin, Heidelberg, **2012**, 1-309. [Crossref], [Google Scholar], [Publisher]
[12] S.H. Ko, I. Park, H. Pan, C.P. Grigoropoulos, A.P. Pisano, C.K. Luscombe, J.M.J. Fréchet, *Nano Lett.*, **2007**, *7*, 1869–1877. [Crossref], [Google Scholar], [Publisher]
[13] H. Wang, T. Lin, A. Kaynak, *Synth. Met.*, **2005**, *151*, 136–140. [Crossref], [Google Scholar], [Publisher]
[14] B.J. Hwang, K.L. Lee, *Thin Solid Films*, **1996**, *279*, 236–241. [Crossref], [Google Scholar], [Publisher]
[15] H. Karami, M.A. Karimi, S. Haghdar, *Mater. Res. Bull.*, **2008**, *43*, 3054–3065. Crossref], [Google Scholar], [Publisher]
[16] M.M. Kashani-Motlagh, M.K. Mahmoudabad, *J. Solgel. Sci. Technol.*, **2011**, *59*, 106–110. [Crossref], [Google Scholar], [Publisher]
[17] T.J. Wilkinson, D.L. Perry, E. Spiller, P. Berdahl, S.E. Derenzo, M.J. Weber, *MRS Proceedings*, **2001**, 704. [Crossref], [Google Scholar], [Publisher]
[18] L. Hashemi, A. Morsali, *J. Inorg. Organomet. Polym. Mater.*, **2010**, *20*, 856–861. [Crossref], [Google Scholar], [Publisher]
[19] V. Safarifard, A. Morsali, *InorganicaChim. Acta*, **2013**, *398*, 151–157. [Crossref], [Google Scholar], [Publisher]
[20] J. Lian, X. Zhang, H. Zhang, Z. Jiang, J. Zhang, *Mater. Lett.*, **2004**, *58*, 1183–1188. [Crossref], [Google Scholar], [Publisher]
[21] W. Feng, E. Sun, A. Fujii, H. Wu, K. Niihara, K. Yoshino, *Bull. Chem. Soc. Jpn.*, **2000**, *73*, 2627–2633. [Crossref], [Google Scholar], [Publisher]
[22] L.M. Yee, H.N.M.E. Mahmud, A. Kassim, W.M.M. Yunus, *Synth. Met.*, **2007**, *157*, 386–389. [Crossref], [Google Scholar], [Publisher]
[23] A. Robin, G.A.S. Martinez, P.A. Suzuki, *Mater. Des.*, **2012**, *34*, 319–324. [Crossref], [Google Scholar], [Publisher]
[24] J. Jang, K. Sim, *Polymer*, **1997**, *38*, 4043–4048. [Crossref], [Google Scholar], [Publisher]
[25] J. Jang, J. Won, *Polymer*, **1998**, *39*, 4335–4342. [Crossref], [Google Scholar], [Publisher]
[26] W.J. Bae, W.H. Jo, Y.H. Park, *Macromol. Res.*, **2002**, *10*, 145–149. [Crossref], [Google Scholar], [Publisher]
[27] L. Burgio, R.J. Clark, S. Firth, *Analyst*, **2001**, *126*, 222-227. [Crossref], [Google Scholar], [Publisher]
[28] D.L. De Faria, S. Venâncio Silva, M.T. De Oliveira, *J. Raman Spectrosc.*, **1997**, *28*, 873-878. [Crossref], [Google Scholar], [Publisher]
[29] Y.M. Choi, H. Lim, H.N. Lee, Y.M. Park, J.S. Park, H.J. Kim, *Biosensors*, **2020**, *10*, 111. [Crossref], [Google Scholar], [Publisher]
[30] S.N. Rafic, S.M.H. Al-Jawad, M.M. Muhsen, *ANJS*, **2017**, *20*, 91–98. [Crossref], [Google Scholar], [Publisher]
[31] X. Song, H. Gong, S. Yin, L. Cheng, C. Wang, Z. Li, Z. Liu, *Adv. Funct. Mater.*, **2013**, *24*, 1194–1201. [Crossref], [Google Scholar], [Publisher]
[32] N.J. Vickers, *Curr. Biol.*, **2017**, *27*, R713–R715. [Crossref], [Google Scholar], [Publisher]

How to cite this article: Ahmed K. Abass*, Wadhah Naji Jassim Al Sieadi, Abdul Karim M.A. Al-Sammarraie. Investigation of the electrical, compositional, and magnetic features of hybrid lead oxide nanocomposites. *Eurasian Chemical Communications*, 2022, 4(11), 1044-1053.
Link: http://www.echemcom.com/article_151319.html